LANGMUIR

Article

pubs.acs.org/Langmuir

Unimer-Assisted Exfoliation for Highly Concentrated Aqueous Dispersion Solutions of Single- and Few-Layered van der Waals Materials

Changbong Yeon,[†,‡] Inyeal Lee,[§] Gil-Ho Kim,[§] and Sun Jin Yun*[,†,‡]

[†]ICT Materials & Components & Research Laboratory, Electronics and Telecommunications Research Institute, 218 Gajeongno, Yuseong-gu, Daejeon 305-700, Republic of Korea

[‡]Department of Advanced Device Engineering, University of Science and Technology, 217 Gajeongno, Yuseong-gu, Daejeon 305-350, Republic of Korea

[§]School of Electronic and Electrical Engineering and Sungkyunkwan Advanced Institute of Nanotechnology (SAINT), Sungkyunkwan University, Suwon 16419, Republic of Korea

Supporting Information

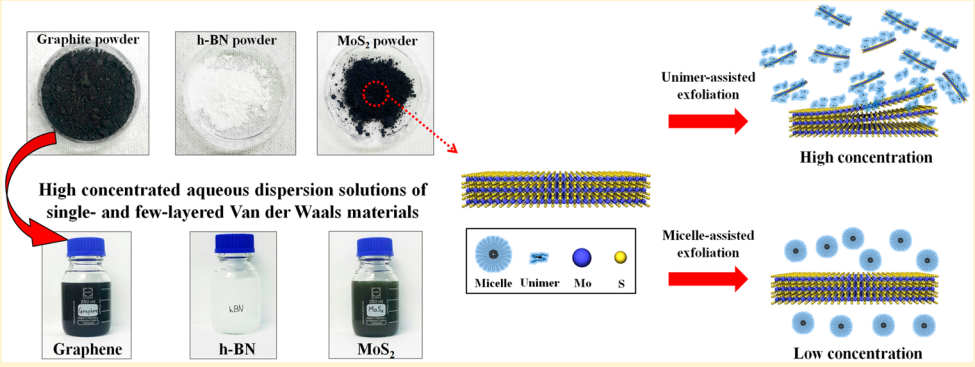

ABSTRACT: We suggest a unimer-assisted exfoliation method for the exfoliation of van der Waals two-dimensional (2D) materials such as graphene, MoS_2, and h-BN and show that the micellar size is a critical parameter for enhancing the exfoliation efficiency. To explain the effectiveness of the unimers in the exfoliation, the influence of the micellar size of a biocompatible block copolymer, Pluronic F-68, is evaluated in view of the yield and thickness of exfoliated 2D flakes. By the addition of water-soluble alcohols, the surfactants exist in the form of a unimer, which facilitates the intercalation into the layered materials and their exfoliation. The results showed that the high exfoliation efficiency could be achieved by controlling the micellar size mostly to be unimers; the average yield rate of MoS_2 exfoliation was 4.51% per hour, and the very high concentration of 1.45 mg/mL was obtained by sonication for 3 h. We also suggested the dielectrophoresis technique as a method for forming a film composed of 2D flakes for diverse applications requiring electrical signals. The unimer-assisted exfoliation method will be substantially utilized to achieve highly concentrated aqueous dispersion solutions of 2D materials.

1. INTRODUCTION

Since graphene was first exfoliated using Scotch tape in 2004, research on van der Waals two-dimensional (2D) materials of the graphene family, transition-metal dichalcogenides (TMDs), and oxides has been focused on their production and applications.[1−4] Single- and few-layer TMDs such as MoS_2, WS_2, and WSe_2 as well as the graphene family exhibiting distinctive physicochemical, electrical, and biological properties have received substantial attention for potential applications in catalysis, biomedicine, sensors, energy storage, thermal management, electronics, and optoelectronics.[5−14] However, the practical application of 2D materials is still limited by the lack of cost-effective and high-yield production methods.

The liquid exfoliation from bulk materials has been investigated because liquid-phase production is a cost-effective method in terms of scaling up compared to vacuum and high-temperature processes such as transition-metal sulfurization and chemical vapor deposition.[15,16] Recently, chemical or electrochemical exfoliation methods in liquid have been intensively studied, but these methods deteriorate the electrical and chemical properties.[17,18] One of the simplest liquid exfoliation methods not accompanying the chemical reaction is sonication-assisted exfoliation in suitable organic solvents or aqueous solution.[19−23] Among them, preparation methods based on an aqueous solution have been generally preferred to those using organic solvents in view of protecting the natural environment

Received: November 15, 2016
Revised: January 12, 2017
Published: January 18, 2017

DOI: 10.1021/acs.langmuir.6b04121
Langmuir 2017, 33, 1217−1226

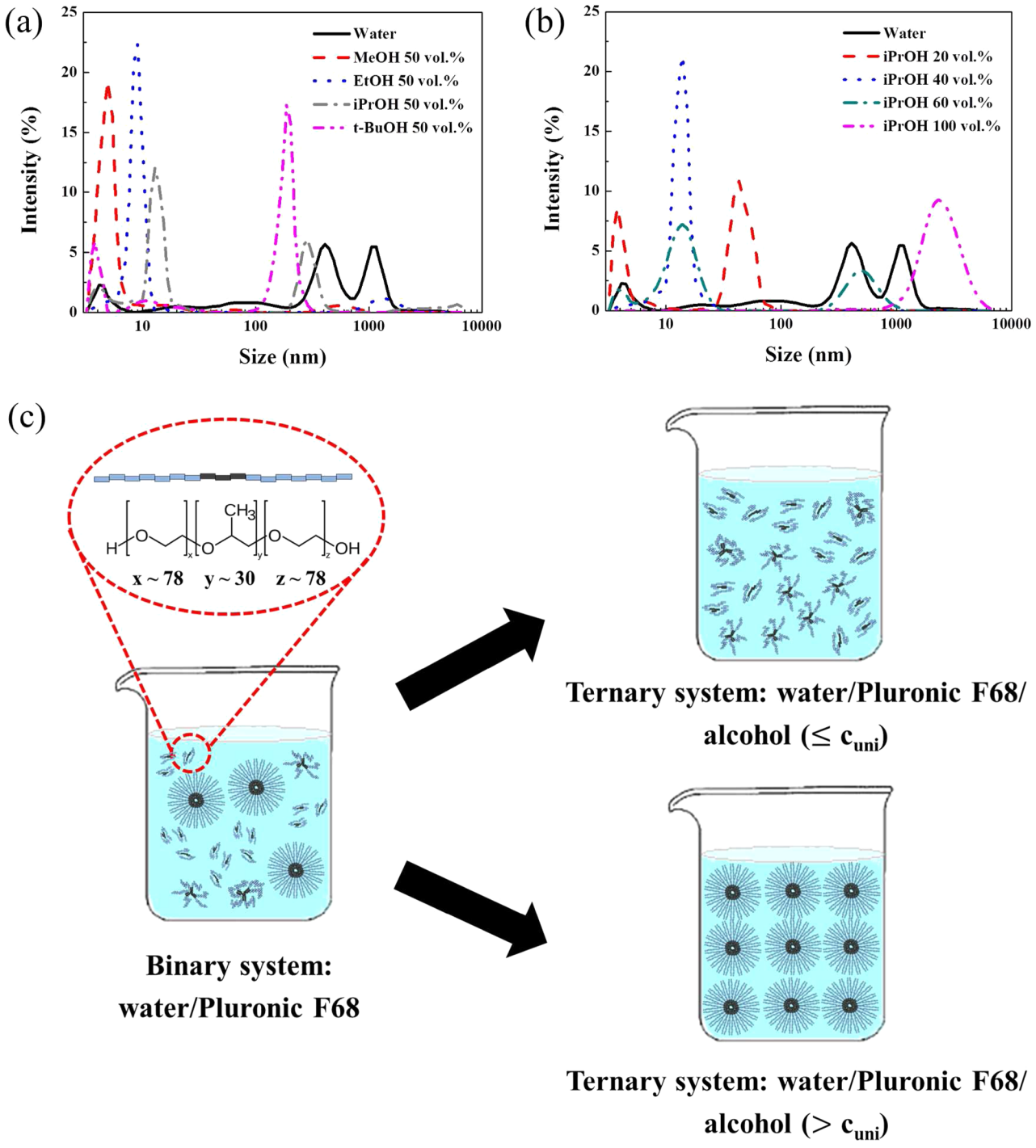

Figure 1. Size distribution of unimers and micelles determined by DLS for (a) 50 vol % alcohols and (b) 0, 20, 40, 60, and 100 vol % iPrOH. (c) Schematics of F-68 molecules in a binary system and ternary systems with different alcohol concentrations (top, $\leq c_{uni}$; bottom, $> c_{uni}$).

and a myriad of applications such as electronic, electrochemical, and biological applications. For the exfoliation of 2D materials in an aqueous solution, dispersing agents such as ionic and nonionic surfactants are necessary because of their hydrophobicity. Ionic and nonionic surfactants can stably disperse 2D materials owing to electrostatic repulsion and steric stabilization effects, respectively. It was reported that nonionic poly(ethylene oxide)-poly(propylene oxide)-poly(ethylene oxide) (PEO-PPO-PEO) triblock copolymer, known by the trade name of Pluronic (which is generally used as one of the ingredients of cosmetics and pharmaceuticals), is effective for the exfoliation of 2D materials.[24] Furthermore, the functionalization of 2D flakes with PEO-PPO-PEO triblock copolymer reduces the toxicity in vitro and in vivo and promotes the safe use of 2D nanoflakes for industrial and biomedical applications.[25,26] The PEO-PPO-PEO copolymers form spherical micelles because of their self-assembling nature in an aqueous solution when the solution concentration exceeds the critical micelle concentration (CMC).[27,28] Above the CMC, the micellar size increases with the surfactant concentration, which leads to an increase in the average number of polymer chains per micelle.[29,30]

DOI: 10.1021/acs.langmuir.6b04121
Langmuir 2017, 33, 1217−1226

One of the important issues in research on the exfoliation of 2D materials in an aqueous solution is to increase the exfoliation yield. However, the effect of changing the micellar size on the exfoliation efficiency of 2D materials has not been investigated in detail. In our previous report, we showed that sodium dodecyl sulfate (SDS) monomer was much more effective for the exfoliation of graphene than large SDS micelles.[31] In this study, we suggest that the micellar size of a polymeric surfactant is very closely related to the exfoliation efficiency and the thickness of exfoliated flakes. The micellar size is affected by many factors including the PPO/PEO ratio, the molecular weight of copolymers, and additives.[32,33] As additives, water-soluble alcohols such as methyl alcohol (MeOH), ethyl alcohol (EtOH), isopropyl alcohol (iPrOH), and *tert*-butyl alcohol (*t*-BuOH) were used in the present work, and their effects on the size of the triblock copolymer $[(EO)_{78}(PO)_{30}(EO)_{78}]$ ((average molecular weight 8400, denoted by Pluronic F-68 (or simply F-68 hereafter)) were systematically investigated by dynamic light scattering (DLS) measurements. The present work elucidating the effect of micellar size was carried out for the exfoliation of MoS_2, graphene, and h-BN, which is currently attracting great interest. We also carried out a dielectrophoresis (DEP) process to form an electrically connected active layer composed of 2D flakes exfoliated in this work. The DEP technique has been generally employed in forming films of microparticles for clinical and biotechnological applications.[34]

2. EXPERIMENTAL DETAILS

2.1. Preparation of Graphene, MoS_2, and h-BN Dispersion Solutions. Graphite (<150 μm, Sigma-Aldrich), molybdenum disulfide (MoS_2, <6 μm, Sigma-Aldrich), and boron nitride (h-BN, <8 μm, Zero Friction-Ecopharos Inc.) powders were used as the starting materials in this work. Triblock copolymer $[(EO)_{78}(PO)_{30}(EO)_{78}]$ of F-68 and alcohols was purchased from Sigma-Aldrich and Dongwoo Fine-Chem, respectively. All of the chemical reagents were used without further purification.

The exfoliation of graphite, MoS_2, and h-BN was carried out using surfactant-assisted sonication. The solution was prepared by the addition of F-68 and alcohols such as MeOH, EtOH, iPrOH, and *t*-BuOH. The CMC of F-68 is 0.04 mM at 25 °C, and the concentration of F-68 ranged from 0.2 to 2.0 mM. The initial concentration of 2D materials was 10 mg/mL. After sonication (Daihan WUC-D06H, 665W, 40 kHz), the dispersion solutions were centrifuged (Hanil combi-514R) at 2000 or 4000 rpm for 15 min to sediment aggregated large flakes. Then, approximately 60% of the supernatant was collected as the final dispersion solution.

2.2. Sample Characterization. The concentration of the dispersion solution was measured using the Lambert−Beer law ($A = \alpha Cl$, where A is the absorbance at 600 nm for MoS_2, 660 nm for graphene, and 300 nm for h-BN; α is the absorption coefficient; C is the concentration; and l is the length of the light path). In accordance with previous reports concerning the exfoliation of MoS_2, graphene, and h-BN, the values of α were set as 2104, 1390, and 2367 mL/mg·m, respectively.[24,35] The yield was defined as the ratio between the weight of dispersed 2D materials and that of the starting material.

The DEP process was carried out to form a film composed of exfoliated MoS_2 flakes. A function generator (Infiniium MSO8064A, Agilent Technologies) was used to create a sinusoidal potential difference. The ac output voltage was monitored by a digital oscilloscope (Agilent 33220A, Agilent Technologies). A droplet of MoS_2 dispersion solution (0.1 μL) was placed between two electrodes. The thicknesses of Au and Ti electrodes were 50 and 5 nm, respectively, deposited by e-beam evaporation. After the DEP process, the sample was rinsed in deionized water (DIW) to remove all remaining traces of the colloidal solution. The current−voltage (I−V) characteristics of the samples formed by DEP were measured by using a Keithley 4200-semiconductor characterization system.

The hydrodynamic diameter of F-68 was measured at 25 °C with a DLS particle size analyzer (UAP-150, Microtrac). An exfoliated 2D dispersion was drop-cast on a thermally grown, 300-nm-thick SiO_2 film on a Si substrate for characterization. The films of 2D flakes were prepared by vacuum filtration on the porous aluminum oxide membrane (Anodisc, Whatman) to obtain SEM images (SEM, S-4800, Hitachi) along with Raman and PL spectra (514 nm, Aramis, Horiba Jobin Yvon) of flakes. The sample for TEM (JEM-2100F, JEOL Ltd.) was prepared by placing a droplet of a colloid suspension on a lacey-carbon Cu grid (LC300-Cu, Electron Microscopy Sciences). To determine the thermal decomposition temperature of F-68, thermal gravimetric analysis (TGA, Mettler Toledo) was carried out from room temperature to 700 °C at a heating rate of 10 °C/min in an N_2 atmosphere. Atomic force microscopy (AFM, XE-100, Park System) was performed to measure the thickness of exfoliated flakes. The zeta-potential values of MoS_2, graphene, and h-BN were measured with a Zetasizer (Nano-Z90, Malvern Instruments). The resistance was obtained from the current−voltage curve measured using a probe station equipped with a source meter (4200-SCS, Keithley).

3. RESULTS AND DISCUSSION

We investigated the effect of the addition of MeOH, EtOH, iPrOH, and *t*-BuOH on the micellar size (i.e., diameter) using DLS as shown in Figure 1a. The concentrations of alcohols and F-68 were 50 vol % and 2.0 mM, respectively. With no alcohol, F-68 existed in the forms of unimers (~4 nm), micelles (~51 nm), and clusters of micelles (>379 nm). The size distribution of micelles was consistent with data from the literature reporting that unimers (~5 nm), large micelles (~90 nm), and clusters (~350 nm) of F-68 coexisted in 1.0 mM F-68 aqueous solution.[30] The unimer was defined as a single molecule in the literature.[30] In this work, when 50 vol % MeOH, EtOH, iPrOH, and *t*-BuOH were added to 2.0 mM F-68 solution, micellar sizes of 5, 8, 13, and 183 nm were mainly detected, respectively, as highlighted with bold font in Table 1.

Table 1. Micellar Sizes Measured in Aqueous Solutions of F-68 (2.0 mM) with MeOH, EtOH, iPrOH, and *t*-BuOH

solvents (vol %)	diameter (nm)	intensity (%)
water (100)	1046, 379, 51, 4	34, 40, 16, 10
MeOH (50)	529, **5**	5, **95**
EtOH (50)	1287, 11, **8**	10, 3, **87**
iPrOH (50)	3732, 276, **13**, 4	6, 29, **57**, 8
t-BuOH (50)	**183**, 7	**80**, 20
iPrOH (20)	**42**, 6, 4	**68**, 5, 27
iPrOH (40)	**13**	**100**
iPrOH (50)	3732, 276, **13**, 4	6, 29, **57**, 8
iPrOH (60)	478, **13**, 4	30, **65**, 5
iPrOH (100)	**2285**	**100**

It was reported that MeOH and EtOH in an aqueous solution of the $(EO)_{100}(PO)_{65}(EO)_{100}$ triblock copolymer acted as water-structure breakers suppressing the micellization of the copolymer whereas *n*-butyl alcohol acted as a water-structure maker promoting micellization.[36] The micellar size is thought to increase with the alkyl chain length of the alcohols added to the F-68 aqueous solutions. We then investigated the effect of alcohol concentration on the micellar size. In the case of iPrOH, F-68 existed in the forms of unimers and small micelles at a concentration lower than 40 vol %. Large micelles were formed at concentrations higher than 40 vol %, and only very large micelles were found at 100 vol % iPrOH as shown in

DOI: 10.1021/acs.langmuir.6b04121
Langmuir 2017, 33, 1217−1226

Figure 1b. The highest concentrations of alcohols (c_{uni}), in which unimers and small micelles are mainly formed, are different because the effectiveness of adding alcohol on reducing the surface tension of a solution varies depending on the alkyl chain length of the alcohol.[37−39] For example, the addition of iPrOH more dramatically reduces the surface tension of the aqueous solution than do MeOH and EtOH.[31,37−39] On the basis of the surface tension of a 40 vol % iPrOH aqueous solution (26 mN/m), we guess that c_{uni} of MeOH, EtOH, and *t*-BuOH would be 78, 66, and 20 vol %, respectively, providing the same surface tension values. The schematics shown in Figure 1c demonstrate that F-68 molecules in a ternary system (water/F-68/alcohol) exist in the form of a unimer or large micelles depending on the concentration of alcohol whereas the unimers and micelles coexist in a binary system (water/F-68).

We found that the addition of alcohol causing the change in micellar size is much more effective for the exfoliation of 2D materials compared to increasing the F-68 concentration (Figure S1). Therefore, the exfoliation of MoS_2 was performed in 2.0 mM F-68 aqueous solutions with different concentrations of alcohols. As shown in Figure 2a, without an alcohol, the average exfoliation yield was less than 0.27% in 2.0 mM F-68 aqueous solution in which micellar sizes of 1046, 379, 51, and 4 nm were detected. In contrast, the average yield was as high as 3.94% in a 30 vol % iPrOH aqueous solution. It then rapidly decreased with increasing concentration from 40 vol %, which is consistent with the changes in micellar size. The highest exfoliation yield was 4.54% that could be obtained in a 50 vol % EtOH aqueous solution in which 8 nm unimers mainly existed, which was 16.8 times higher than the value (0.26%). These results indicate that high-yield exfoliation can be achieved under conditions where unimers and small micelles mainly exist. The yield was linearly increased as the sonication time increased, as shown in Figure 2b and Table S1. The average yield rate of MoS_2 calculated by a linear curve fitting was 4.51% per hour, which was much higher than the value (0.77% per hour) from a recent report of high-yield exfoliation of MoS_2 in an aqueous solution. (We calculated the yield rate using the reported data in the linearly increasing region with sonication time.[40])

The number of unimers or micelles (the effective number of surfactant molecules) is inversely proportional to the aggregation number of surfactants under a constant concentration of surfactant in an aqueous dispersion solution. According to the universal force-field modeling of the direct exfoliation of graphene sheets, the adsorption of surfactants on graphene strongly affects the exfoliation process.[46,47] The surfactants in the aqueous solution with no alcohols tend to generate large micelles and are less likely to adsorb on the surface of flakes compared to those with an alcohol. Thus, the smaller micellar size of polymeric surfactant is a critical parameter for achieving a higher exfoliation efficiency because of the larger effective number of surfactant molecules adsorbed on the surface of the flake as illustrated in Figure 2c.

We observed pronounced spectral changes depending on the type of alcohols and the concentration of iPrOH, demonstrating how the micellar size affects the exfoliation of 2D materials as plotted in Figure 3a,b. Backes et al. introduced a simple method to characterize dispersions of liquid-exfoliated MoS_2 flakes and reported that the energy of the A-excitons and the relative intensity of the B-excitonic transition varied with the thickness and size of the flakes whereas the absorption

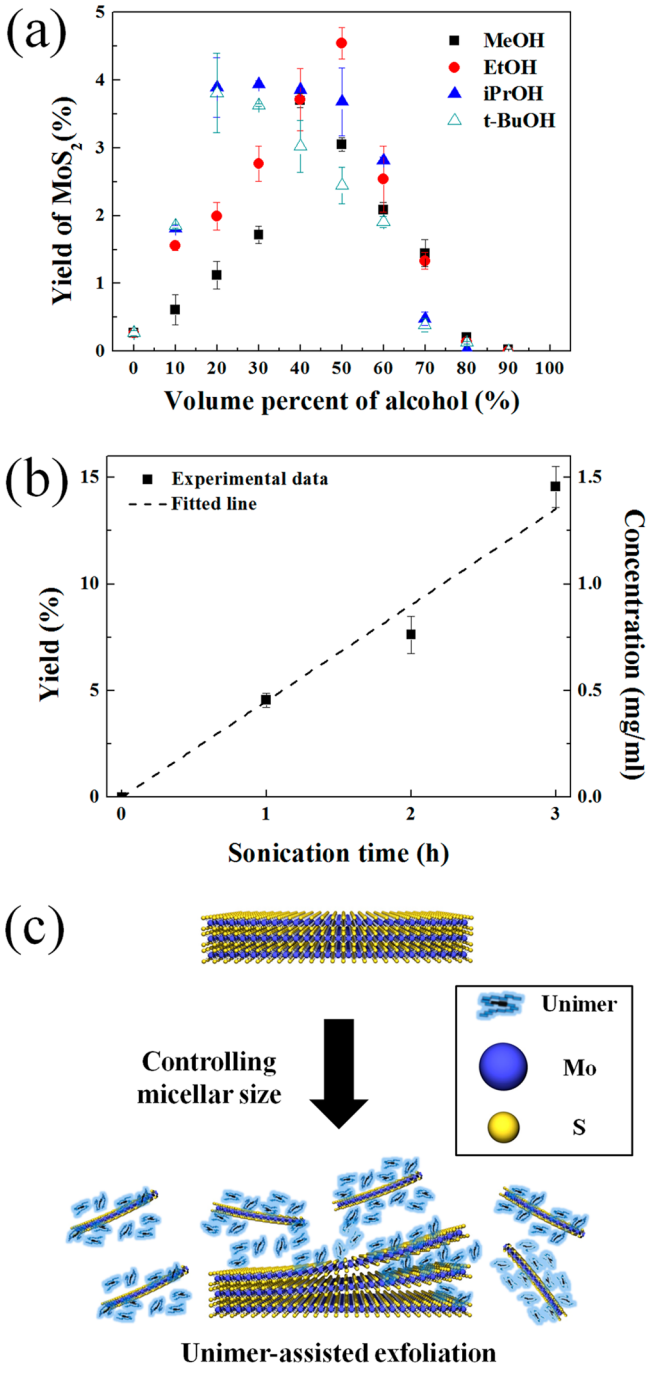

Figure 2. (a) Average yield of MoS_2 flakes exfoliated in water/F-68/MeOH (■), EtOH (red ●), iPrOH (blue ▲), and *t*-BuOH (Δ) solutions with different volume percentages of the alcohols. (b) Changes in the average yield and concentration of MoS_2 exfoliated in a 50 vol % EtOH aqueous solution as a function of sonication time. The fitted line is indicated with a corresponding dotted line. (c) Schematic of unimer exfoliation of MoS_2 flakes.

coefficient at 345 nm is widely independent of the thickness and size.[40] Thus, the change in the peak of the A-excitons, λ_A, which is determined by the second derivative of the absorption spectra (Figure S2), is clear evidence for estimating the changes in thickness and size of the exfoliated MoS_2 flakes; the blue shift of λ_A indicates that the exfoliated MoS_2 flakes become smaller and thinner whereas the red shift shows that the exfoliated MoS_2 flakes become larger and thicker. The λ_A without any

DOI: 10.1021/acs.langmuir.6b04121
Langmuir 2017, 33, 1217−1226

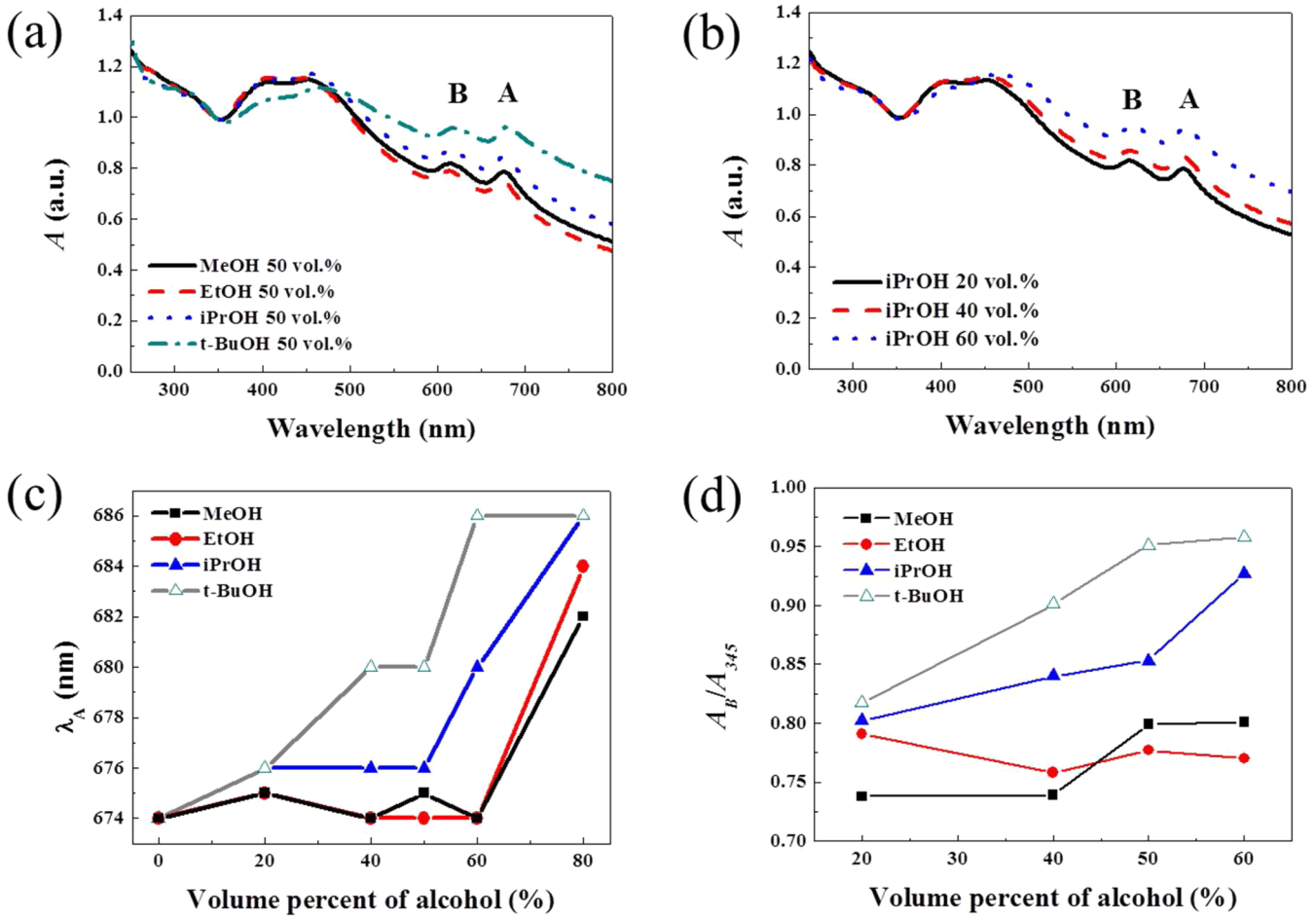

Figure 3. Absorption spectra, normalized at 345 nm, of MoS_2 dispersions exfoliated with (a) 50 vol % alcohols and (b) 20, 40, and 60 vol % iPrOH. The peaks of the A- and B-excitons are marked. (c) λ_A and (d) A_B/A_{345} plotted as functions of the volume percent of alcohols.

alcohols was 674 nm, and it remains almost constant until 60 vol % of MeOH and EtOH, and increased to 682 and 684 nm at 80 vol % of MeOH and EtOH, respectively, as shown in Figure 3c. In the case of iPrOH and *t*-BuOH, λ_A starts to increase even with the small addition of 20 vol %. This indicates that the thickness and the size of exfoliated MoS_2 flakes are larger than those of flakes exfoliated using short-chain alcohols such as MeOH and EtOH. Figure 3d indicates that the considerable increase in the ratio of absorbance at the B-excitonic peak (605 nm) to that at the local minimum at 345 nm, A_B/A_{345}, with increasing concentration of alcohols also indicated that the thickness and size became larger.

For achieving a high concentration of an atomically thin MoS_2 dispersion, the exfoliation utilizing the size-controlled F-68 molecules was performed for 3 h and centrifuged at 4000 rpm for 15 min. The photograph of this MoS_2 dispersion with a concentration of ~1 mg/mL was shown in the inset of Figure 4a. From the absorption spectra in Figure 4a, the values of λ_A and A_B/A_{345} were 666 nm and 0.36, respectively, which clearly indicate that the exfoliated MoS_2 flakes are very thin.[41] The flakes were obtained by filtration through the porous aluminum oxide membrane to observe the size of the exfoliated flakes by SEM. The SEM image shows both MoS_2 flakes and membrane pores as indicated by blue and red arrows in Figure 4b. Exfoliated MoS_2 flakes were thin enough to see the membrane pores through the flakes and most of the lateral sizes were ≤ 1 μm. The TEM image clearly shows that the MoS_2 flake is atomically thin as shown in Figure 4c. The selective area electron diffraction (SAED) pattern in the inset of Figure 4c also shows that the exfoliated MoS_2 is a single crystal in hexagonal structure. Using the same method as applied in a previous report,[31] the thickness of exfoliated MoS_2 flakes was measured from AFM images of ~180 flakes on a mica substrate. Figure 4d shows a histogram of the number of layers of MoS_2 flakes that can be calculated by dividing the measured thickness by the thickness of a MoS_2 single layer, approximately 0.7 nm. These results indicated that bulk MoS_2 was successfully exfoliated into single- and few-layered MoS_2 flakes by a unimer-assisted method.

We performed PL measurements for bulk and exfoliated MoS_2 flakes. It was reported that monolayer MoS_2 shows a strong PL peak at ~1.79 eV corresponding to the direct band gap emission.[42,43] As shown in Figure 5a, for the bulk MoS_2 film, any strong PL peaks were not observed because it is an indirect band gap (~1.2 eV) material. Thin MoS_2 flakes showed a strong PL peak at ~1.78 eV after water-washing, although a weak PL intensity was observed before water-washing. This result indicates that the surfactant of F-68 can be easily removed by water-washing because PEO parts of F-68 physically adsorbed on 2D flakes oriented toward the water, and the surfactant removal is essential for applications such as optoelectronic applications.

Raman spectroscopy was also used to investigate the change in vibrational energy of MoS_2 flakes by exfoliation and

DOI: 10.1021/acs.langmuir.6b04121
Langmuir 2017, 33, 1217−1226

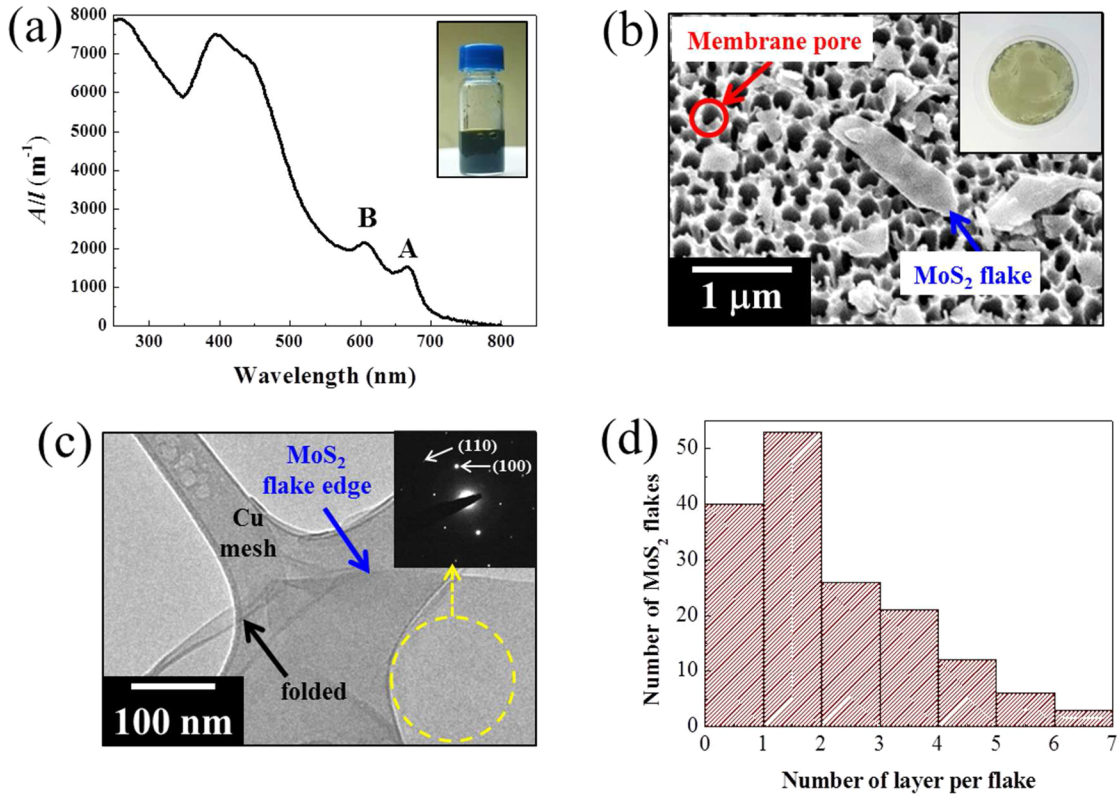

Figure 4. (a) Absorption spectra of the MoS_2 dispersion exfoliated in the solution where the 8 nm unimers dominantly existed. The inset is a photograph of a MoS_2 dispersion obtained by sonication for 3 h and centrifugation for 15 min at 4000 rpm. (b) SEM image of the exfoliated MoS_2 flakes on an aluminum oxide membrane. The inset shows the photograph after vacuum filtration of the MoS_2 dispersion solution on an aluminum oxide membrane. (c) TEM image of the exfoliated MoS_2 flakes on a lacey-carbon Cu grid. The inset is the SAED pattern corresponding to the yellow circle. (d) Histogram of the number of layers of MoS_2 flakes measured from AFM images.

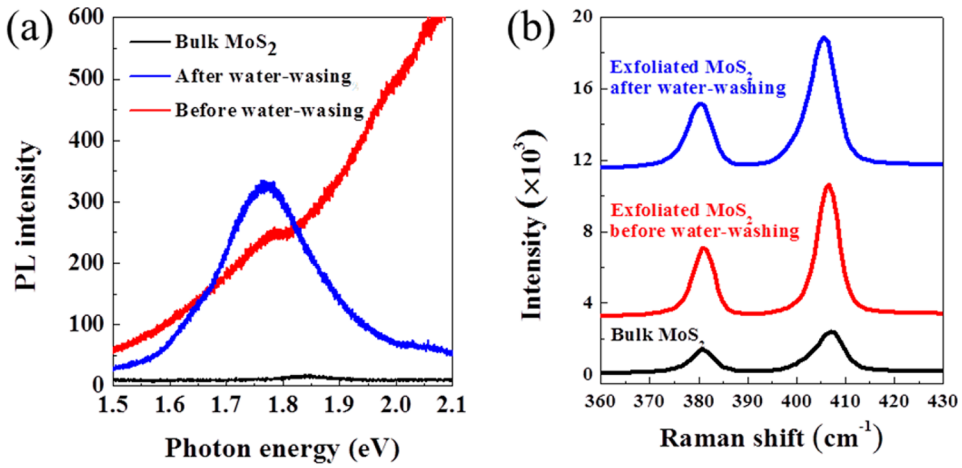

Figure 5. (a) PL and (b) Raman spectra of the bulk MoS_2 and exfoliated MoS_2 flakes before and after water-washing.

subsequent water-washing. There are four first-order Raman-active modes, A_{1g}, $E_{2g}{}^1$, $E_{2g}{}^2$, and E_{1g}, of bulk 2H-MoS_2.[44] Among them, Figure 5b showed two strong vibrational modes of in-plane $E_{2g}{}^1$ and out-of-plane A_{1g} (Figure S3). For bulk 2H-MoS_2, the frequencies of $E_{2g}{}^1$ and A_{1g} were 381 and 407 cm^{-1}, respectively. It was reported that the Raman peaks of MoS_2 (A_{1g} and $E_{2g}{}^1$ modes) shift away from each other in frequency with increasing thickness.[48] However, as shown in Figure 5b, the Raman peak differences between A_{1g} and $E_{2g}{}^1$ for the bulk MoS_2 and the exfoliated MoS_2 were 25.9 and 25.3 cm^{-1}, respectively, which showed a slight difference. The reason might be due to the film preparation method for the measurement of Raman spectra. The films were fabricated by vacuum filtration and contained flakes having different thicknesses as illustrated in Figure 4d. Thus, the Raman peak shift depending on the thickness of the flake could not be seen clearly, which is consistent with the earlier report using the vacuum filtration method.[49] The Raman peak intensities of exfoliated flakes significantly increased compared to those of bulk MoS_2. The frequency of the A_{1g} peak also showed a red shift, which can be explained using the van der Waals force model.[44,45] The red shift of the A_{1g} peak indicated that the

DOI: 10.1021/acs.langmuir.6b04121
Langmuir 2017, 33, 1217−1226

restoring force between interlayer S−S bonds decreased as the interaction between the layers decreased in a few layered exfoliated flakes compared to the bulk MoS_2. For the sample before water-washing, the degree of red shift was smaller than for the water-washed sample because of physically adsorbed F-68 on the flakes.

The surfactant of F-68 can also be removed by thermal decomposition (Figure S4). The 2D flakes can remain stable after the thermal decomposition process because the thermal decomposition temperature of F-68 was as low as 235 °C. Using the graphene flakes, resistances (R) were measured after the annealing processes at 250, 350, and 450 °C to indirectly confirm the surfactant removal on 2D flakes. As a result, R was significantly decreased by a factor of 463.5 with the thermal decomposition process even at 250 °C (Figure S5). As demonstrated above, the optical and electrical properties could be well recovered by removing surfactants from exfoliated 2D flakes via a simple subsequent process.

We further exfoliated graphite and h-BN in the same manner. As shown in Figure 6a, the concentration of EtOH for the highest exfoliation yield was 50 vol %, at which unimers mainly exist; the yields of graphene and h-BN were 1.83 and 0.85%, respectively (Figure S6). The results clearly demonstrate that unimers and small micelles are much more effective for the exfoliation of other 2D materials compared to large micelles.

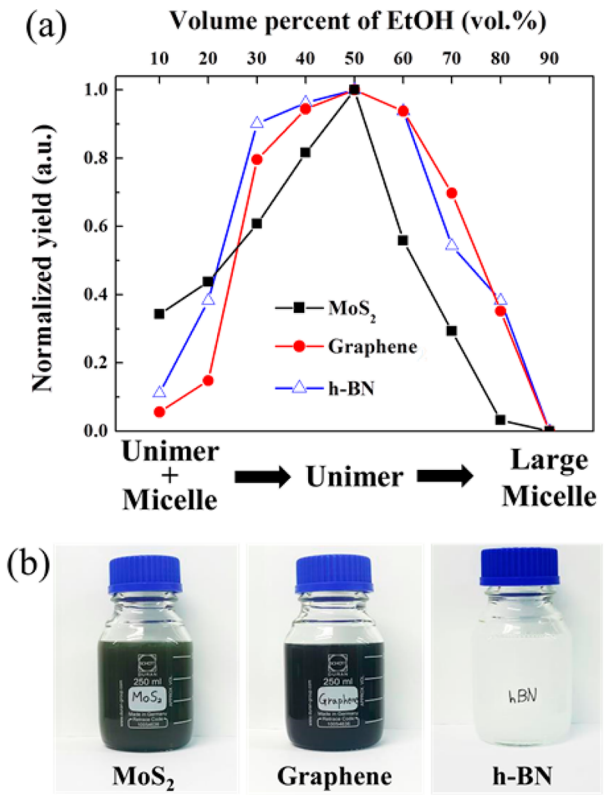

Figure 6. (a) Normalized yield of MoS_2 (■), graphene (red ●), and h-BN (blue Δ) exfoliated in water/F-68/EtOH as a function of EtOH concentration. Inset: schematics of F-68 molecules in a ternary system with different concentrations of EtOH. (b) Photographs of MoS_2, graphene, and h-BN dispersion solutions in 250 mL bottles, taken after storing for 6 months.

The dispersion solutions of MoS_2, graphene, and h-BN exfoliated by unimers and small micelles remain very stable even after 6 months as shown in Figure 6b. The 2D flakes coated by F-68 can be stabilized not only by steric stabilization but also by partially electrostatic interactions. As shown in Figure S7, the zeta-potential values of MoS_2, graphene, and h-BN dispersion solutions are −15.7, −22.9, and −24.4 mV, respectively, which are consistent with earlier reported values using nonionic surfactant.[50,51] This result confirms that the aqueous solution of 2D materials exfoliated by F-68 unimers is kinetically stable over a large period of time.

The parallel assembly of 2D flakes should be performed to utilize 2D flakes for the electronic applications such as biosensor and gas sensor. In this work, we successfully deposited MoS_2 flakes between two electrodes using the DEP method. The system for DEP assembly is schematically depicted in Figure 7a. The assembly of exfoliated MoS_2 flakes was driven by the DEP force, which can be defined as

$$F_{DEP} = (p\cdot\nabla)E = (v\tilde{a}E\cdot\nabla)E \quad (1)$$

where p is the effective dipole moment, v is the volume of the particle, and $\tilde{a}$ is the complex effective polarizability.[52] According to eq 1, F_{DEP} is dependent on the gradient of the nonuniform electric field and the polarizability of the particle, and the deposition parameters depend on the size and thickness. In this work, we successfully deposited MoS_2 flakes using the DEP method followed by dipping in DIW and showed the optical microscope image in Figure 7b. The I−V characteristic curve for the MoS_2 film formed by DEP is linear as shown in Figure 7c. The resistance of the MoS_2 film formed by DEP was approximately ∼5.0 × 10^8 Ω. In the case of unsuccessful deposition, no sheets at all are observed, and its I−V curve is nonlinear. When the thickness of MoS_2 is increased, the frequency of the E_{2g}^1 mode decreases while the frequency of the A_{1g} mode increases.[44] Figure 7d shows that the frequency difference between two modes was 24.4 cm^{-1}, which corresponded to four layers.

4. CONCLUSIONS

We first clarified the effect of micellar size on the exfoliation of van der Waals 2D materials such as MoS_2, graphene, and h-BN, and the exfoliation efficiency could be greatly increased by controlling the micellar size mostly to be unimers of F-68 by adding water-soluble alcohols including MeOH, EtOH, iPrOH, and t-BuOH. With the addition of alcohols at a concentration lower than c_{uni}, F-68 existed in the forms of unimers or very small micelles whereas unimers, micelles, and large clusters of micelles coexisted in an F-68 aqueous solution with no alcohols. The present work demonstrated that the smaller micellar size of the polymeric surfactant could result in a higher exfoliation efficiency commonly observed for 2D materials owing to a larger effective number of surfactant molecules adsorbed on the surface of the flake. The exfoliation yield could be enhanced by 16.8 times by controlling the size of the polymeric surfactants. We also successfully formed a film composed of MoS_2 flakes between two electrodes using the DEP technique. The effective and facile methodology proposed in this work should be useful for understanding the exfoliation of 2D materials and achieving high-concentration 2D dispersion solutions that can be utilized as precursor solutions for the DEP process. We believe that this work allows 2D flakes to be successfully utilized for electronic applications.

DOI: 10.1021/acs.langmuir.6b04121
Langmuir 2017, 33, 1217−1226

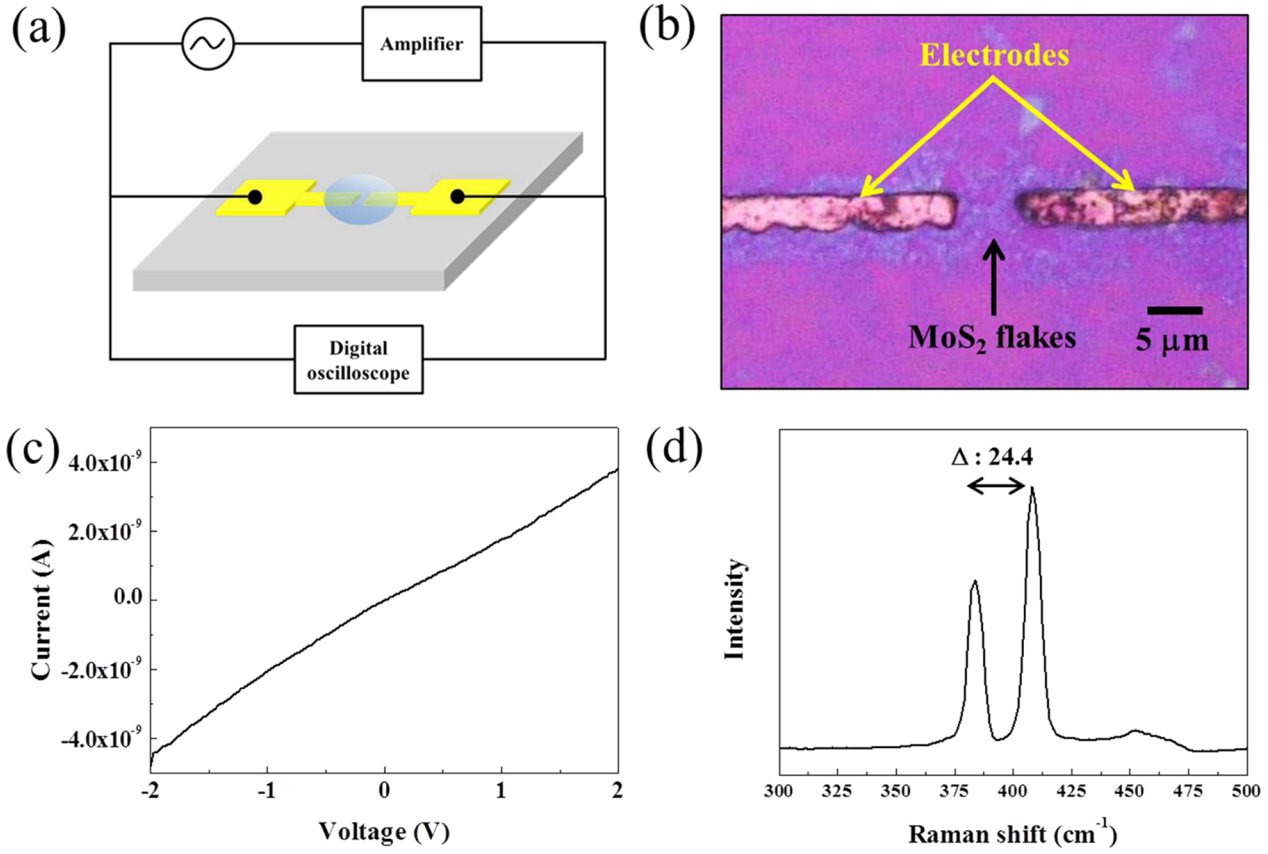

Figure 7. (a) Schematic diagram of the experimental setup for DEP assembly. (b) Optical microscope image of the MoS_2 film formed by the DEP method. (c) *I*–*V* curve and (d) Raman spectra for the MoS_2 film.

■ ASSOCIATED CONTENT

Supporting Information

The Supporting Information is available free of charge on the ACS Publications website at DOI: 10.1021/acs.langmuir.6b04121.

Change in the yield of graphene flakes as a function of the concentration of F-68 with different iPrOH concentrations. Second derivative spectra of the normalized absorption peaks for MoS_2 dispersion exfoliated in F-68 aqueous solutions with different alcohols. Atomic displacement vectors of the E_{2g}^1 and A_{1g} vibrational modes, as viewed along the [100] direction. Thermogravimetric plot of graphene exfoliated in F-68 aqueous solution. Resistance of graphene flakes with respect to the annealing temperature. Average yield of MoS_2, graphene, and h-BN exfoliated in water/F-68/EtOH as a function of EtOH concentration. Zeta potential spectra for F-68-stabilized MoS_2, graphene, and h-BN. Yield of MoS_2 exfoliated in a 50 vol % EtOH aqueous solution of F-68 with increasing sonication time. (PDF)

■ AUTHOR INFORMATION

Corresponding Author

*E-mail: sjyun@etri.re.kr.

ORCID

Sun Jin Yun: 0000-0002-3665-0393

Notes

The authors declare no competing financial interest.

■ ACKNOWLEDGMENTS

This work was supported by an Institute for Information & Communications Technology Promotion (IITP) grant funded by the Korean government (MSIP) (B0117-16-1003, Fundamental Technologies of Two-Dimensional Materials and Devices for the Platform of New-Functional Smart Devices).

■ REFERENCES

(1) Novoselov, K. S.; Jiang, D.; Schedin, F.; Booth, T. J.; Khotkevich, V. V.; Morozov, S. V.; Geim, A. K. Two-dimensional atomic crystals. *Proc. Natl. Acad. Sci. U. S. A.* **2005**, *102*, 10451−10453.

(2) Novoselov, K. S.; Geim, A. K.; Morozov, S. V.; Jiang, D.; Zhang, Y.; Dubonos, S. V.; Grigorieva, I. V.; Firsov, A. A. Electric field effect in atomically thin carbon films. *Science* **2004**, *306*, 666−669.

(3) Geim, A. K.; Grigorieva, I. V. Van der Waals heterostructures. *Nature* **2013**, *499*, 419−425.

(4) Wang, X.; Feng, H.; Wu, Y.; Jiao, L. Controlled synthesis of highly crystalline MoS_2 flakes by chemical vapor deposition. *J. Am. Chem. Soc.* **2013**, *135*, 5304−5307.

(5) Lukowski, M. A.; Daniel, A. S.; Meng, F.; Forticaux, A.; Li, L. S.; Jin, S. Enhanced hydrogen evolution catalysis from chemically exfoliated metallic MoS_2 nanosheets. *J. Am. Chem. Soc.* **2013**, *135*, 10274−10277.

(6) Zhu, W. J.; Low, T.; Lee, Y. H.; Wang, H.; Farmer, D. B.; Kong, J.; Xia, F.; Avouris, P. Electronic transport and device prospects of monolayer molybdenum disulphide grown by chemical vapour deposition. *Nat. Commun.* **2014**, *5*, 3087.

(7) Stephenson, T.; Li, Z.; Olsen, B.; Mitlin, D. Lithium ion battery applications of molybdenum disulfide (MoS_2) nanocomposites. *Energy Environ. Sci.* **2014**, *7*, 209−231.

(8) Tan, C.; Yu, P.; Hu, Y.; Chen, J.; Huang, Y.; Cai, Y.; Luo, Z.; Li, B.; Lu, Q.; Wang, L.; Liu, Z.; Zhang, H. High-yield exfoliation of

DOI: 10.1021/acs.langmuir.6b04121
Langmuir 2017, 33, 1217−1226

ultrathin two-dimensional ternary chalcogenide nanosheets for highly sensitive and selective fluorescence DNA sensors. *J. Am. Chem. Soc.* **2015**, *137*, 10430−10436.
(9) Lu, J. P.; Lu, J. H.; Liu, H. W.; Liu, B.; Chan, K. X. H.; Lin, J.; Chen, W.; Loh, K. P.; Sow, C. H. Improved photoelectrical properties of MoS_2 films after laser micromachining. *ACS Nano* **2014**, *8*, 6334−6343.
(10) Chen, Y.; Tan, C.; Zhang, H.; Wang, L. Two-dimensional graphene analogues for biomedical applications. *Chem. Soc. Rev.* **2015**, *44*, 2681−2701.
(11) Perkins, F. K.; Friedman, A. L.; Cobas, E.; Campbell, P. M.; Jernigan, G. G.; Jonker, B. T. Chemical vapor sensing with monolayer MoS_2. *Nano Lett.* **2013**, *13*, 668−673.
(12) Renteria, J. D.; Nika, D. L.; Balandin, A. A. Graphene thermal properties: applications in thermal management and energy storage. *Appl. Sci.* **2014**, *4*, 525−547.
(13) Shahil, K. M. F.; Balandin, A. A. Graphene-multilayer graphene nanocomposites as highly efficient thermal interface materials. *Nano Lett.* **2012**, *12*, 861−867.
(14) Malekpour, H.; Chang, K.-H.; Chen, J.-C.; Lu, C.-Y.; Nika, D. L.; Novoselov, K. S.; Balandin, A. A. Thermal conductivity of graphene laminate. *Nano Lett.* **2014**, *14*, 5155−5161.
(15) Coleman, J. N.; Lotya, M.; O'Neill, A.; Bergin, S. D.; King, P. J.; Khan, U.; Young, K.; Gaucher, A.; De, S.; Smith, R. J.; Shvets, I. V.; Arora, S. K.; Stanton, G.; Kim, H.; Lee, K.; Kim, G. T.; Duesberg, G. S.; Hallam, T.; Boland, J. J.; Wang, J. J.; Donegan, J. F.; Grunlan, J. C.; Moriarty, G.; Shmeliov, A.; Nicholls, R. J.; Perkins, J. M.; Grieveson, E. M.; Theuwissen, K.; McComb, D. W.; Nellist, P. D.; Nicolosi, V. Two-dimensional nanosheets produced by liquid exfoliation of layered materials. *Science* **2011**, *331*, 568−571.
(16) Paton, K. R.; Varrla, E.; Backes, C.; Smith, R. J.; Khan, U.; O'Neill, A.; Boland, C.; Lotya, M.; Istrate, O. M.; King, P.; Higgins, T.; Barwich, S.; May, P.; Puczkarski, P.; Ahmed, I.; Moebius, M.; Pettersson, H.; Long, E.; Coelho, J.; O'Brien, S. E.; McGuire, E. K.; Sanchez, B. M.; Duesberg, G. S.; McEvoy, N.; Pennycook, T. J.; Downing, C.; Crossley, A.; Nicolosi, V.; Coleman, J. N. Scalable production of large quantities of defect-free few-layer graphene by shear exfoliation in Liquids. *Nat. Mater.* **2014**, *13*, 624−630.
(17) Yin, Y.; Han, J.; Zhang, Y.; Zhang, X.; Xu, P.; Yuan, Q.; Samad, L.; Wang, X.; Wang, Y.; Zhang, Z.; Zhang, P.; Cao, X.; Song, B.; Jin, S. Contributions of phase, sulfur vacancies, and edges to the hydrogen evolution reaction catalytic activity of porous molybdenum disulfide nanosheets. *J. Am. Chem. Soc.* **2016**, *138*, 7965−7972.
(18) Zheng, J.; Zhang, H.; Dong, S.; Liu, Y.; Nai, C. T.; Shin, H. S.; Jeong, H. Y.; Liu, B.; Loh, K. P. High yield exfoliation of two-dimensional chalcogenides using sodium naphthalenide. *Nat. Commun.* **2014**, *5*, 2995.
(19) Cao, M.; Wang, N.; Wang, L.; Zhang, Y.; Chen, Y.; Xie, Z.; Li, Z.; Pambou, E.; Li, R.; Chen, C.; Pan, F.; Xu, H.; Penny, J.; Webster, J. R. P.; Lu, J. R. Direct exfoliation of graphite into graphene in aqueous solutions of amphiphilic peptides. *J. Mater. Chem. B* **2016**, *4*, 152−161.
(20) Pan, L.; Liu, Y.-T.; Xie, X.-M.; Ye, X.-Y. Facile and green production of impurity-free aqueous solutions of WS_2 nanosheets by direct exfoliation in water. *Small* **2016**, *12*, 6703.
(21) Parviz, D.; Irin, F.; Shah, S. A.; Das, S.; Sweeney, C. B.; Green, M. J. Challenges in liquid phase exfoliation, processing, and assembly of pristine graphene. *Adv. Mater.* **2016**, *28*, 8796.
(22) Tran, T. S.; Park, S. J.; Yoo, S. S.; Lee, T.-R.; Kim, T. Y. High shear-induced exfoliation of graphite into high quality graphene by Taylor-Couette flow. *RSC Adv.* **2016**, *6*, 12003−12008.
(23) Bindhu, B.; Sharu, B. K.; Gopika, M. S.; Praseetha, P. K.; Veluraja, K. Molybdenum disulfide nanoflakes through Li-AHA assisted exfoliation in an aqueous medium. *RSC Adv.* **2016**, *6*, 22026−22033.
(24) Mansukhani, N. D.; Guiney, L. M.; Kim, P. J.; Zhao, Y.; Alducin, D.; Ponce, A.; Larios, E.; Yacaman, M. J.; Hersam, M. C. High-concentration aqueous dispersions of nanoscale 2D materials using nonionic, biocompatible block copolymers. *Small* **2016**, *12*, 294−300.
(25) Wang, X.; Mansukhani, N. D.; Guiney, L. M.; Ji, Z.; Chang, C. H.; Wang, M.; Liao, Y.-P.; Song, T.-B.; Sun, B.; Li, R.; Xia, T.; Hersam, M. C.; Nel, A. E. Differences in the toxicological potential of 2D versus aggregated molybdenum disulfide in the lung. *Small* **2015**, *11*, 5079−5087.
(26) Jastrzebska, A. M.; Kurtycz, P.; Olszyna, A. R. Recent advances in graphene family materials toxicity investigations. *J. Nanopart. Res.* **2012**, *14*, 1320.
(27) Malmsten, M.; Lindman, B. Self-assembly in aqueous block copolymer solutions. *Macromolecules* **1992**, *25*, 5440−5445.
(28) Glatter, O.; Scherf, G. Characterization of a poly(ethylene oxide)-poly(propylene oxide) triblock copolymer(EO_{27}-PO_{39}-EO_{27}) in aqueous solution. *Macromolecules* **1994**, *27*, 6046−6054.
(29) Olea, A. F.; Carrasco, H.; Espinoza, L.; Acevede, B. Solubilization of p-alkylphenols in Puronics F-68 and F-127 micelles: partition coefficients and effect of solute on the aggregate structure. *J. Chil. Chem. Soc.* **2014**, *59*, 2451−2454.
(30) Ghaouar, N.; Henda, M. B.; Aschi, A.; Gharbi, A. Study of PEO-PPO-PEO copolymers conformational changes: viscosity and dynamic light scattering measurements. *J. Macromol. Sci., Part B: Phys.* **2011**, *50*, 2150−2164.
(31) Yeon, C.; Yun, S. J.; Lee, K.; Lim, J. W. High-yield graphene exfoliation using sodium dodecyl sulfate accompanied by alcohols as surface-tension-reducing agents in aqueous solution. *Carbon* **2015**, *83*, 136−143.
(32) Bahadur, P.; Pandya, K. Aggregation behavior of Pluronic P-94 in water. *Langmuir* **1992**, *8*, 2666−2670.
(33) Alexandridis, P.; Holzwarth, J. F.; Hatton, T. A. Micellization of poly(ethylene oxide)-poly(propylene oxide)-poly(ethylene oxide) triblock copolymers in aqueous solutions: thermodynamics of copolymer association. *Macromolecules* **1994**, *27*, 2414−2425.
(34) Pethig, R. Review article-dielectrophoresis: status of the theory, technology, and applications. *Biomicrofluidics* **2010**, *4*, 022811.
(35) Ge, Y.; Wang, J.; Shi, Z.; Yin, J. Gelatin-assisted fabrication of water-dispersible graphene and its inorganic analogues. *J. Mater. Chem.* **2012**, *22*, 17619−17624.
(36) Kwon, K.; Park, M. J.; Hwang, J.; Char, K. Effects of alcohol addition on gelation in aqueous solution of poly(ethylene oxide)-poly(propylene oxide)-poly(ethylene oxide) triblock copolymer. *Polym. J.* **2001**, *33*, 404−410.
(37) Vazquez, G.; Alvarez, E.; Navaza, J. M. Surface tension of alcohol + water from 20 to 50 °C. *J. Chem. Eng. Data* **1995**, *40*, 611−614.
(38) Huy, N. T.; Maeda, A.; Uyen, D. T.; Trang, D. T. X.; Sasai, M.; Shiono, T.; Oida, T.; Harada, S.; Kamei, K. Alcohols induce beta-hematin formation via the dissociation of aggregated heme and reduction in interfacial tension of the solution. *Acta Trop.* **2007**, *101*, 130−138.
(39) Cheong, W. J.; Carr, P. W. The surface tension of mixtures of methanol acetonitrile, tetrahydrofuran, isopropanol, tertiary butanol and dimethylsulfoxide with water at 25 °C. *J. Liq. Chromatogr.* **1987**, *10*, 561−581.
(40) Guan, G.; Zhang, S.; Liu, S.; Cai, Y.; Low, M.; Teng, C. P.; Phang, I. Y.; Cheng, Y.; Duei, K. L.; Srinivasan, B. M.; Zheng, Y.; Zhang, Y.; Han, M. Protein induces layer-by-layer exfoliation of transition metal dichalcogenides. *J. Am. Chem. Soc.* **2015**, *137*, 6152−6155.
(41) Backes, C.; Smith, R. J.; McEvoy, N.; Berner, N. C.; McCloskey, D.; Nerl, H. C.; O'Neill, A.; King, P. J.; Higgins, T.; Hanlon, D.; Scheuschner, N.; Maultzsch, J.; Houben, L.; Duesberg, G. S.; Donegan, J. F.; Nicolosi, V.; Coleman, J. N. Edge and confinement effects allow in situ measurement of size and thickness of liquid-exfoliation nanosheets. *Nat. Commun.* **2014**, *5*, 4576.
(42) Nan, H.; Wang, Z.; Wang, W.; Liang, Z.; Lu, Y.; Chen, Q.; He, D.; Tan, P.; Miao, F.; Wang, X.; Wang, J.; Ni, Z. Strong photoluminescence enhancement of MoS_2 through defect engineering and oxygen bonding. *ACS Nano* **2014**, *8*, 5738−5745.

DOI: 10.1021/acs.langmuir.6b04121
Langmuir 2017, 33, 1217−1226

(43) Eda, G.; Yamaguchi, H.; Voiry, D.; Fujita, T.; Chen, M. W.; Chhowalla, M. Photoluminescence from chemically exfoliated MoS_2. *Nano Lett.* **2011**, *11*, 5111−5116.
(44) Ye, M.; Winslow, D.; Zhang, D.; Pandey, R.; Yap, Y. K. Recent advancement on the optical properties of two-dimensional molybdnum disulfide (MoS_2) thin films. *Photonics* **2015**, *2*, 288−307.
(45) Liu, N.; Kim, P.; Ye, J. H.; Kim, S.; Lee, C. J. Large-area atomically thin MoS_2 nanosheets prepared using electrochemical exfoliation. *ACS Nano* **2014**, *8*, 6902−6910.
(46) Pupysheva, O. V.; Farajian, A. A.; Knick, C. R.; Zhamu, A.; Jang, B. Z. Modeling direct exfoliation of nanoscale graphene platelets. *J. Phys. Chem. C* **2010**, *114*, 21083−21087.
(47) Zhao, J.; Wang, Z.; Zhao, Q.; Xing, B. Adsorption of phenanthrene on multilayer graphene as affected by surfactant and exfoliation. *Environ. Sci. Technol.* **2014**, *48*, 331−339.
(48) Yao, Y.; Tolentino, L.; Yang, Z.; Song, X.; Zhang, W.; Chen, Y.; Wong, C.-P. High-Concentration Aqueous Dispersions of MoS_2. *Adv. Funct. Mater.* **2013**, *23*, 3577−3583.
(49) Smith, R. J.; King, P. J.; Lotya, M.; Wirtz, C.; Khan, U.; De, S.; O'Neill, A.; Duesberg, G. S.; Grunlan, J. C.; Moriaty, G.; Chen, J.; Wang, J.; Minett, A. I.; Nicolosi, V.; Coleman, J. N. Large-Scale Exfoliation of Inorganic Layered Compounds in Aqueous Surfactant Solutions. *Adv. Mater.* **2011**, *23*, 3944−3948.
(50) Smith, R. J.; Lotya, M.; Coleman, J. N. The importance of repulsive potential barriers for the dispersion of graphene using surfactants. *New J. Phys.* **2010**, *12*, 125008.
(51) White, B.; Banerjee, S.; O'Brien, S.; Turro, N. J.; Herman, I. P. Zeta-potential measurements of surfactant-wrapped individual single-walled carbon nanotubes. *J. Phys. Chem. C* **2007**, *111*, 13684−13690.
(52) Burg, B. R.; Schneider, J.; Maurer, S.; Schirmer, N. C.; Poulikakos, D. Dielectrophoretic integration of single- and few-layer graphenes. *J. Appl. Phys.* **2010**, *107*, 034302.

DOI: 10.1021/acs.langmuir.6b04121
Langmuir 2017, 33, 1217−1226